A proposal of a hybrid tuber structure with a steel reinforced concrete wall-column and steel beam

T. Sagawa[1], D. Ishii[1], S. Sakamoto[1], H. Ito[2], K. Fukuda[2] & Y. Ichinohe[2]
[1]*Shimizu Corporation, Japan*
[2]*Nippon Steel and Sumitomo Metal Corporation, Japan*

Abstract

The authors proposed the hybrid tuber structure with steel reinforced concrete wall-column and steel beam in order to realize a versatile space in a building. The peripheral frame in this structure consists of a steel reinforced concrete wall-column and a peripheral steel beam just embedded to the wall-column, resulting in a rigid connection. In the orthogonal direction of the peripheral frame, a long spanned steel beam is rigidly connected by welding to the H-shaped steel inside the wall-column. This paper investigates the bearing stress transfer mechanism in the in-plane direction of the wall-column. A total number of seven beam-column joint specimens, in half scale of the actual structure, were tested under cyclic loading to simulate the seismic loads. The test parameters include the width and depth, and the embedded length of the steel beam. Based on experimental knowledge, the authors propose the design formula for the structure in terms of the ultimate strength and bearing capacity of concrete.
Keywords: hybrid structure, steel beam, steel reinforced concrete wall-column, cyclic loading, bearing fracture, bearing stress transfer mechanism.

1 Introduction

The authors proposed the hybrid tuber structure with steel reinforced concrete wall-column and steel beam in order to realize a versatile space in a building. Figure 1 shows the overview of the hybrid structure, and fig. 2 shows the steel reinforced concrete wall-column and steel beam. The peripheral frame in this

WIT Transactions on The Built Environment, Vol 152, © 2015 WIT Press
www.witpress.com, ISSN 1743-3509 (on-line)
doi:10.2495/ERES150231

structure consists of the steel reinforced concrete (SRC) wall-column and the peripheral steel beam merely embedded to the wall-column, resulting in a rigid connection. In the orthogonal direction of the peripheral frame, a long spanned steel beam is rigidly connected by welding to the H-shaped steel column inside the wall-column. This paper investigates the bearing stress transfer mechanism in the in-plane direction of the wall-column.

Figure 3 shows the plastic hinge formation mechanism of the hybrid tuber structure and normal steel frame building. In the hybrid tuber structure, the entire plastic hinge is designed to be formed in steel beams, and also the base of SRC wall-columns is designed so as to behave as a steel column. Story deformation in the hybrid tuber structures, because of the high rigidly of SRC wall-columns, can be almost equalized all over the stories during earthquakes. Moreover the seismic energy absorbed by the steel beams of each story can suppress the maximum response drift. While, in the conventional steel frame buildings the

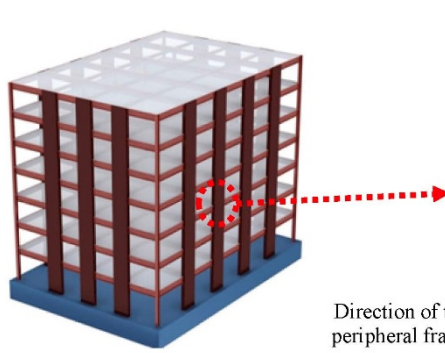

Figure 1: Overview of hybrid tuber structure.

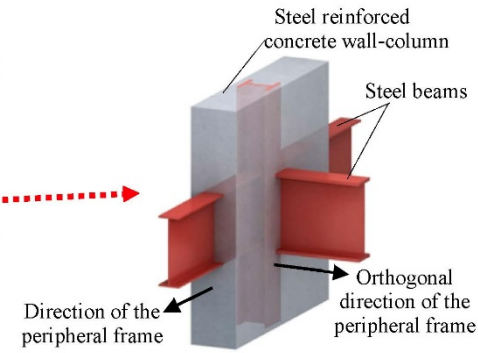

Figure 2: Steel reinforced concrete wall-column and steel beam.

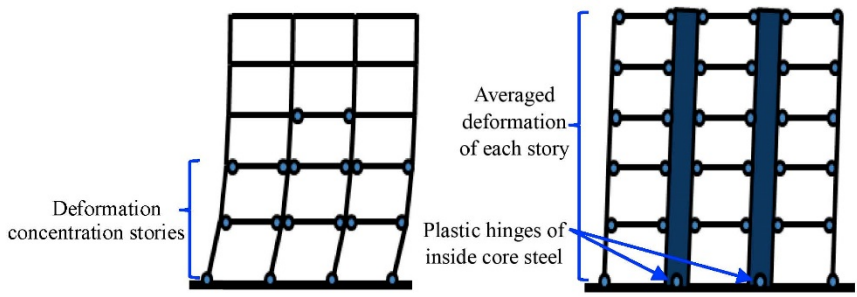

Figure 3: Plastic hinge formation mechanisms. (a) Conventional steel frame; (b) Hybrid tuber building.

story deformation may be concentrated at the lower stories. Thus, this building has a high seismic performance than conventional steel frame building.
Overview of test programs

1.1 Specimens

A total number of seven beam-column joint specimens were designed in half scale of the actual structure. Five of the specimens represent the interior one-way joints of intermediate floor, and two of the specimens represent the T-shaped joint of top floor. The test parameters include the width and depth, and the embedded length of the steel beam. Details of the specimens are shown in Table 1 and fig. 4. Specimen Nos. 1 and 6 were designed so as to fail in the yielding of steel flange of the beam, and Nos. 2 to 5 to fail in the bearing of concrete of the joint. Specimen No. 7 was designed to fail in upward punching of top concrete, and reduced U-shaped rebar than No. 6.

Concrete was placed vertically in the same manner as in the actual construction. End of the steel beam is connected to the H-shaped steel inside the wall-column with two sets of high-tension bolts (2×M12/F8T), which are temporarily used to simply set the steel before casting concrete in specimens; not used structurally.

Table 1: List of speciments.

Specimens	Type of joint	Steel reinforced concrete wall-column size*1 D_wxB_w (mm)	Steel beam size (mm)	Embedded length of the steel beam (mm)	Failure mode	Test parameters
No.1	Interior joint of intermediate floor	1250x280 (Fc*2 36)	H-400x125 x9x12	575	Yielding of steel flange of beam	Control specimen
No.2		900x280 (Fc27)	H-400x125 x9x12	400	Bearing fracture of concrete	Embedded length of beam
No.3		900x280 (Fc27)	H-400x100 x9x19	400		Column/beam width ratio
No.4		900x280 (Fc27)	H-400x75 x9x19	400		Column/beam width ratio
No.5		1250x280 (Fc27)	H-500x125 x9x22	575		Depth of beam
No.6	T-shaped joint of top floor	1270x280 (Fc36)	H-350x125 x7x11	525	Yielding of steel flange of beam	Control specimen
No.7		1270x280 (Fc36)	H-350x125 x12x19	535	Punching fracture of top concrete	U-shaped rebar

*1: Size of steel inside wall-column: H-175x175x7.5x11(SS400); Longitudinal rebars: 18-D16 and 10-D10(SD345).
*2: Fc: Specified concrete strength, in MPa.

Table 2 shows the mechanical properties of materials used for the specimens. Tests of the compressive strength and static modulus of elasticity for concrete comply with the "JIS A1108 Method of tests for compressive strength of concrete" and "JIS A 1149 Method of test for static modulus of elasticity of concrete". Steel tensile test pieces are fabricated in accordance with "JIS Z 2201 test pieces for tensile test for metallic materials" The tensile test was conducted as specified in "JIS Z 2241 Methods for tensile test for metallic materials". Concrete used for the tests are Fc27 and Fc36. Other materials used for the tests

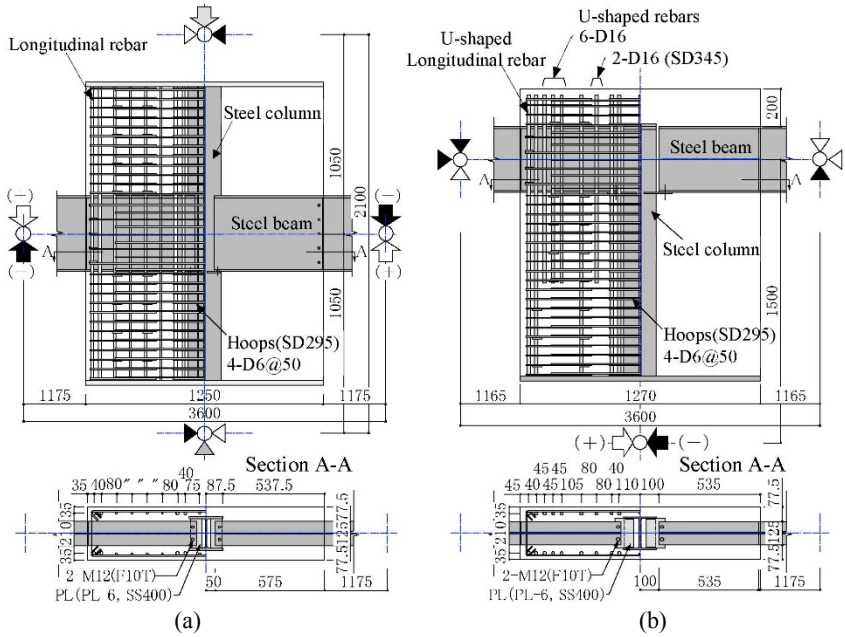

Figure 4: Detail of specimens (dimensions in mm). (a) Specimen No. 1; (b) Specimen No. 6.

Table 2: Mechanical properties of materials.

(a) Concrete

Specimens	Compressive strength (MPa)	Young's modulus (GPa)
No.1	45.4	30.4
No.2	27.1	26.5
No.3	30.2	27.8
No.4	31.1	27.0
No.5	31.3	26.1
No.6	42.4	31.3
No.7	41.0	30.8

(b) Rebar and steel

Parts		Yield strength (MPa)	Young's modulus (GPa)	Remarks
Rebar				
Longitudinal rebar, U-shaped rebar	D16	388	187	Nos.1-5
		396	187	Nos.6,7
Longitudinal rebar	D10	368	173	Nos.1-5
hoops	D6	355	188	Nos.1-5
		355	187	Nos.6,7
Steel beam				
Flange	PL-22	354	200	No.5
	PL-19	359	196	Nos.3,4
		362	202	No.7
	PL-12	356	195	Nos.1,2
	PL-11	366	207	No.6
Web	PL-12	403	199	No.7
	PL-11	376	194	Nos.1,2
		448	195	Nos.3,4
		429	193	No.5
	PL-7	427	207	No.6

include deformed bars D10 and D16 for longitudinal rebars, and D6 for hoops (the numbers refer to the nominal diameter). All specimens have almost the same clear span (1165–1175mm) of beams.

1.2 Testing configuration

Figure 5 shows the loading configuration. In specimens Nos. 1 to 5 the constant axial load of 100kN was applied with a hydraulic jack on top of the wall-column. Cyclic shear loads were asymmetrically applied to the point of assumed contraflexure in each steel beam by 1000kN compression-tension hydraulic jacks, controlling the vertical deformation angle of each steel beam so as to be equal to the story angle *R* as defined in fig. 6. In order to prevent steel beams from lateral buckling at the larger deformation, out-of-plane bracings are placed under the beam.

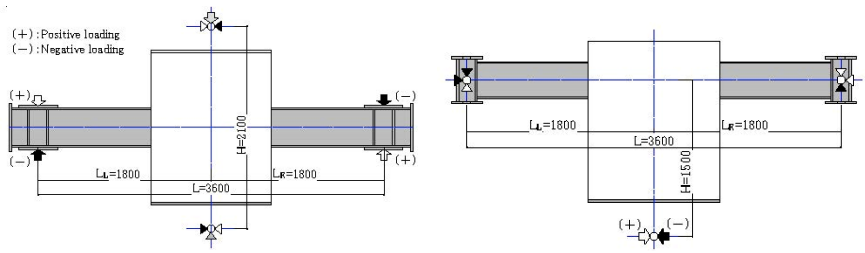

(a) (b)

Figure 5: Loading configurations. (a) Specimens Nos. 1 to 5; (b) Specimens Nos. 6 and 7.

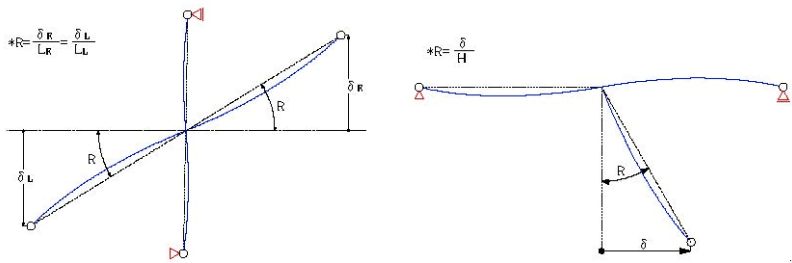

Figure 6: Definition of deformation angle. (a) Specimens Nos. 1 to 5; (b) Specimens Nos. 6 and 7.

As for the specimens Nos. 6 and 7, cyclic horizontal shear loads were applied to the point of assumed contraflexure in the wall-column by 2000kN compression-tension hydraulic jack, controlling the lateral deformation angle so as to the story angle *R* as defined in fig. 6.

The loading cycles consist of first once at R=±0.125, and twice at R=±0.25, ±0.5, ±1.0, ±2.0, ±3.0, ±4.0, ±5.0%rad. respectively, and then up to failure. For specimen No.1, however, the loading cycles at R=±0.5 and ±1.0%rad. were repeated ten times, and for specimen No. 6 R=±1.0%rad. was repeated ten times.

2 Test results

Figure 7 shows the relationships between the average shear force of the left and right beams vs. deformation angle for each specimen.

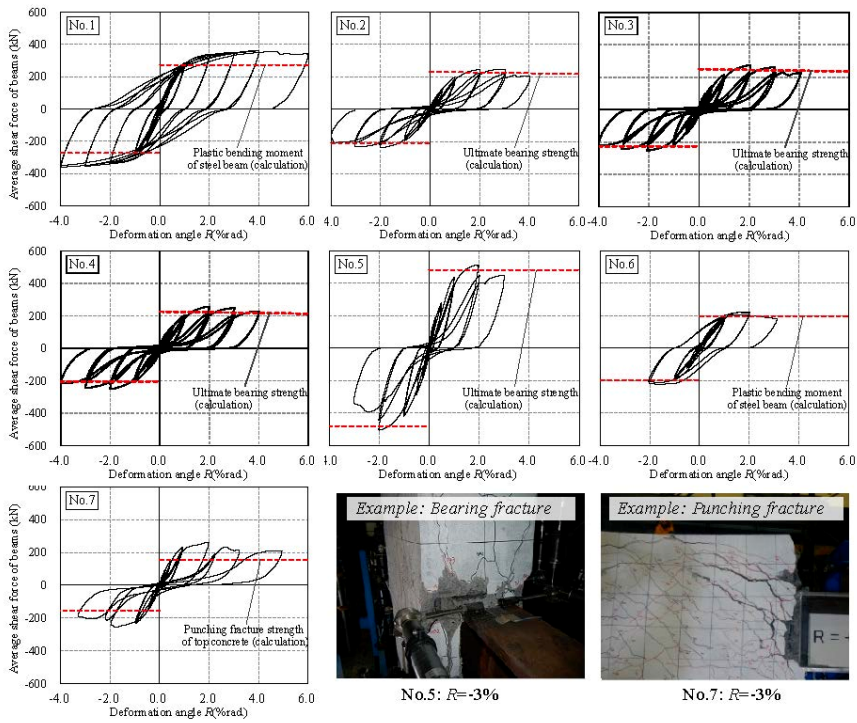

Figure 7: Average shear force of beams vs. deformation angle.

Specimen No. 1: observed cracks in the SRC wall-column at R=+0.25%rad., and experienced yielding of the flange at the starting point of the steel beam embedment at R=+0.7%rad. After the cycles at R=±0.5, ±1.0%rad. repeated ten times, no significant deteriorating crack was found. Moreover the specimen showed the spindle-shaped load vs. deformation relationship, even up to R=+4.0%rad. The ultimate strength was determined by local buckling of the steel beam.

Specimens Nos. 2 to 4: observed cracks in the SRC wall-column at R=+0.25%rad., and experienced yielding of the flange at the starting point of the steel embedment around R=+1.0%rad. Once the ultimate strength reached at

R=+2.0-+3.0%rad., a bearing failure occurred at the top and bottom of the steel embedment with decreasing loads.

Specimen No. 5: observed cracks in the SRC wall-column at *R*=+0.125%rad., and experienced yielding of the flange at the starting point of the steel embedment around *R*=+1.3%rad. Once the ultimate strength reached at *R*=+2.0%rad., a bearing failure occurred at the top and bottom of the steel embedment with decreasing loads. Since a significant decrease in strength was found after *R*=+2.0%rad., test was ended up to at ±3.0%rad. cycle.

Specimen No. 6: observed cracks in the SRC wall-column at *R*=+0.125%rad. and experienced yielding of the flange at the starting point of the steel beam embedment at R=+0.7%rad. Even after the cycles of R=±1.0%rad. repeated ten times, no significant deteriorating crack was found. Moreover the specimen showed the spindle-shaped load vs. deformation relationship until *R*=±2.0%rad., and a significant decrease in strength was found at *R*=+3.0%rad., accompanied local buckling of the steel beam.

Specimen No.7: observed cracks in the SRC wall-column at *R*=+0.125%rad. and experienced flexural yielding of U-shaped rebar at *R*=-1.0%rad. Once the ultimate strength reached at R=+2.0%rad., a punching failure occurred at the top of the concrete with decreasing loads. A significant decrease in strength was found after *R*=+2.0%rad.

3 Proposal of seismic design

3.1 Bearing stress transfer mechanism

The bearing stress transfer mechanism in the in-plane direction of the wall-column is shown in fig. 8.

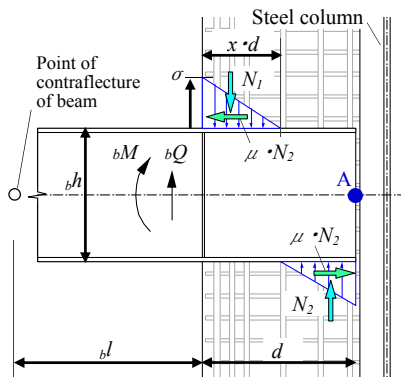

${}_bM$:	Moment of the beam at the starting point of the steel embedment
${}_bQ$:	Shear force of the beam
N_1,N_2:	Bearing resistant forces by the grip mechanism
μ:	Friction coefficient
σ:	Maximum bearing stress of concrete by N_1 ($\sigma = \lambda \cdot \sigma_B$)
λ:	Increase factor of bearing strength of concrete
${}_bb$:	Steel beam flange width
${}_bh$:	Steel beam depth
d:	Embedded length of the steel beam
${}_bl$:	Length from the contraflecture of beam to the outer surface of wall-column
x	Coefficient of bearing shift point

Figure 8: Bearing stress transfer mechanism.

Moment and shear force acting on the beam is modeled based on the grip mechanism by concrete, accompanied by bearing force and friction.

Based on a design for the embedded steel columns in "Recommendation for Design of Connections Steel Structures [1]", the bearing stress distribution acting orthogonally on the embedded steel beam flange is assumed to be linear in the axial direction. Bearing resistant forces N_1, N_2 acting as shown in fig. 8 are expressed by eqns. (1) and (2).

The equilibrium of the exerted forces and moment with respect to a point A (as shown fig. 8) gives the coefficient x of bearing shift point, and consequently ${}_bQ$ shear force of beam. The yield strength of beam-column joint was herein defined as the one when maximum compressive stress of concrete reaches the bearing strength of concrete can be given by eqn. (5). Equation (6): x as referring to the coefficient of bearing shift point of References [2–4].

$$N_1 = \frac{1}{2}\sigma_{\cdot b} b \cdot x \cdot d \ , \ N_2 = \frac{1}{2}\sigma_{\cdot b} b \cdot \frac{(1-x)^2}{x} \cdot d \tag{1), (2}$$

$$\left[\begin{array}{l} {}_bQ \cdot (l+d) = N_1 \cdot \left(1 - \frac{1}{3}x\right) \cdot d - N_2 \cdot \frac{(1-x)}{3} \cdot d + \mu \cdot (N_1 + N_2)_b h \qquad (3) \\ {}_bQ = N_1 - N_2 = \frac{1}{2}\sigma_{\cdot b} b \cdot \frac{2x-1}{x} \cdot d \qquad (4) \end{array} \right.$$

$$\therefore {}_jQ_y = \frac{1}{2}\sigma_{\cdot b} b \cdot \frac{2x-1}{x} \cdot d \ , \quad x = \frac{3l+2d}{6l+3d} + \frac{\mu_{\cdot b} h}{8l+4d} \tag{5), (6}$$

In the T-shaped joint, instead of concrete resistant forces, U-shaped rebar is used to prevent upward punching fracture as illustrated fig. 9. Since U-shaped rebars are expected to ensure the tension as a reaction of the bearing stress capacities, the rebars should not be allowed to yield. Based on the design concept, the contribution of the U-shaped rebars to the beam-column joint strength is expressed by eqns (7)–(10). In case that the joint strength is determined by the yielding of the U-shaped rebar, the punching fracture strength of top concrete can be given by eqns (11) and (12).

$$T_1 \geq N_1 = {}_bQ_u \cdot \frac{x^2}{2x-1} \ , \ T_1 \cdot l_1 \geq N_1 \cdot \frac{2}{3}x \cdot d \tag{7), (8}$$

$$T_2 \geq N_2 = {}_bQ_u \cdot \frac{(1-x)^2}{2x-1} \ , \ T_2 \cdot l_2 \geq N_2 \cdot \frac{2}{3}(1-x) \cdot d \tag{9), (10}$$

$${}_jM_{u1} = \frac{T_1 \cdot l_1}{N_1 \cdot \frac{2}{3}x \cdot d} \cdot {}_bM_u \ , \ {}_jM_{u2} = \frac{T_2 \cdot l_2}{N_2 \cdot \frac{2}{3}(1-x) \cdot d} \cdot {}_bM_u \tag{11), (12}$$

3.2 Shear force distribution of beam

Figure 10 shows the strain measurement locations of specimen No. 5 for steel webs. Figure 11 shows the shear force ratios at R=+0.5%rad., 1.0%rad. respectively for specimens Nos. 5 and 7 as examples. The shear force ratio defined as the ratio of the shear in steel beam divided by the beam shear forces. The shear force in steel beam was calculated by the integral of shear stress distribution at each section with respect to steel depth. The shear stress was calculated by the three-axis wire strain gauges in a section of the steel web.

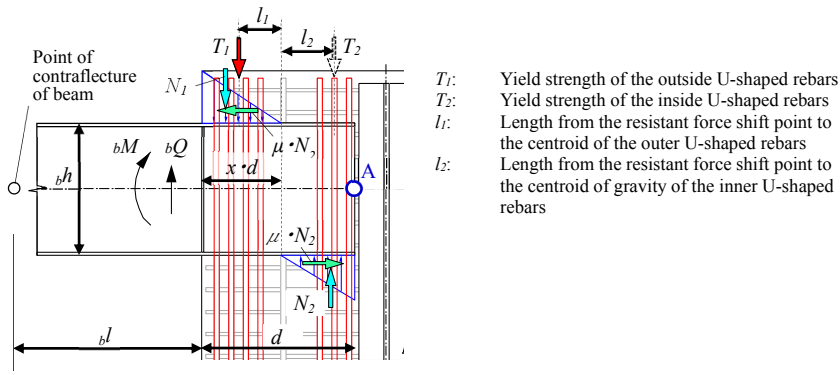

Figure 9: Bearing stress transfer mechanism of top floor.

Figure 11 shows the calculated shear force ratio distribution in comparison with the experimental shear force, where the friction coefficient was taken as 0.4 with Reference [1].

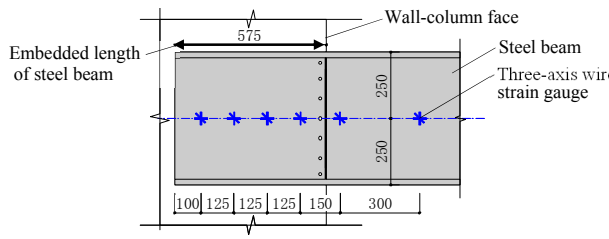

Figure 10: Measurement of locations of strain in steel web.

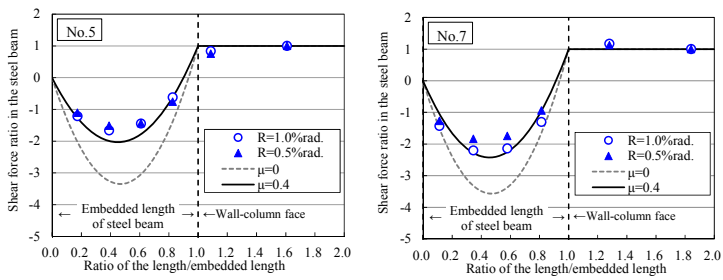

Figure 11: Shear force ratio distribution in steel beam.

3.3 Ultimate bearing strength of concrete

The ultimate strength ${}_jQ_u$ of beam-column joint by taking into the account the bearing stress distribution as a block other than a triangular, can be evaluated 1.5 times the yield strength ${}_jQ_y$. The increase factor λ of bearing strength of concrete is determined from the experimental results of the ultimate strength with bearing fracture. Figure 12 shows the relationship between the factor and the wall-column/beam width ratio. As the beam/wall-column width ratio becomes smaller, the factor increases up to 2.5 linearly. The authors proposed the increase factor evaluation of bearing strength of concrete as in eqn. (13) and fig. 12. The increase factors were evaluated based on the minimum experimental results between the left and right beams.

Moreover, the λ values by eqn. (13) are shown in fig. 12 with test values of the ultimate strength. The coefficients are evaluated using the experimental results of the smaller strength in left and right beams.

$$\lambda = 3.25 - 3.75 \cdot \frac{{}_bb}{{}_wD} \quad \text{where,} \quad 0.27 \le \frac{{}_bb}{{}_wD} \le 0.45 \tag{13}$$

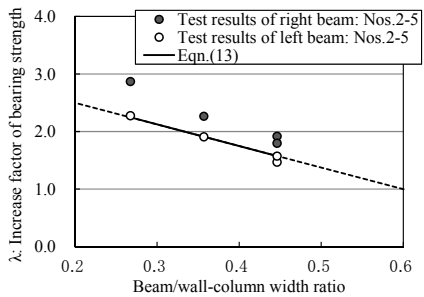

Figure 12: Increase factor of bearing strength of concrete.

3.4 Ultimate strength evaluation

Table 3 shows the comparison of experimental and calculated strengths according to the proposed evaluation in this paper. In this evaluation, the calculated ultimate strength of the steel beam is based on fully plastic moment.

For steel flange yielding type as in specimens Nos. 1 and 5, the bearing fracture type as in specimens Nos. 2 to 5, and for the upward punching fracture type as in specimen No. 7, the experimental ultimate strengths were reasonably consistent with the calculated ones. In calculating punching fracture strength of specimen No. 7, only the tensile strength of the U-shaped rebar is taken into account rather than the concrete; consequently leading to an underestimation the experimental result. It turned out that the proposed ultimate strength evaluation formula in this study is very effective.

Table 3: List of specimens.

Specimens	Experimental maximum average shear force of beams (kN)	Calculated ultimate shear force of beams (kN)		Ratio of (experiment) divided by (calculation)	Failure mode
		Plastic bending of steel beam	Shear force at the bearing fracture*		
1	363	273	656	1.33	Yielding of steel flange of beam
2	247	273	231	1.07	Bearing fracture of the joint
3	272	311	250	1.09	
4	257	256	226	1.14	
5	515	537	482	1.07	
6	223	197	197	1.13	Yielding of steel flange of beam
7	264	365	154	1.71	Punching fracture of top concrete

*Punching fracture of top concrete is included in this category.

4 Conclusions

The authors proposed the hybrid tuber structure with steel reinforced concrete wall-column and steel beam. Tested were the specimens of about half a scale to identify the structural performance of the joint in-plane direction of the wall-column. Based on the test results and the models of bearing stress transfer mechanism, the conclusions are drawn as follows:

1. For the interior one-way joints of intermediate floor and the T-shaped joints of top floor, it was confirmed that the failure modes, such as the yielding of steel flange of the beam and bearing fracture of the joint, could be controlled as expected.
2. The experimental results showed that the ultimate bearing strength of the joint was determined by the bearing strength of concrete and embedded length of the steel beam, consequently it turned out that the ultimate bearing strength of concrete reached 2.5 times the concrete strength.
3. The shear force distribution of the embedded steel beam was estimated properly based on bearing stress transfer mechanism with a friction factor of 0.4.
4. The authors proposed the design formula for the structure in terms of the ultimate strength and bearing capacities of concrete.

References

[1] Architectural Institute of Japan, Recommendation for Design of Connections Steel Structures, 2012 (in Japanese).

[2] Kiyo-omi Kanemoto, Shear capacities for hybrid steel beams jacketed within reinforced concrete ends connected to reinforced concrete columns, Earthquake Resistant Engineering Structures IX, pp. 283–295, 2013.
[3] Shin-ichi Sakamoto, Kentaro Nakagawa, Nobuyuki Maeda, Takashi Kunugi, Yasuo Ichinohe, Koji Fukuda, Hiroshi Ito and Satoru Kitaoka, Development of Smart Tuber Structure with SRC Wall Column and Steel Beam (Part 1) Outline of the Structure and Trial Design, Summaries of Technical Papers of Annual Meeting Architectural Institute of Japan, pp. 1481–1482, 2013 (in Japanese).
[4] Daigo Ishii, Takayuki Sagawa, Shin-ichi Sakamoto, Hiroshi Ito and Satoru Kitaoka, Development of Smart Tuber Structure with SRC Wall Column and Steel Beam (Part 4) Structural Performance of the Beam – Wall Connection of the Wall Width Direction, Summaries of Technical Papers of Annual Meeting Architectural Institute of Japan, pp. 1487–1488, 2013 (in Japanese).